

New polarimetric study of the galactic X-ray burster GX 13+1

Anna Bobrikova¹, Alessandro Di Marco², Fabio La Monaca^{2,3,4}, Juri Poutanen¹, Sofia V. Forsblom¹, and Vladislav Loktev¹

¹ Department of Physics and Astronomy, FI-20014 University of Turku, Finland
e-mail: anna.a.bobrikova@utu.fi

² INAF Istituto di Astrofisica e Planetologia Spaziali, Via del Fosso del Cavaliere 100, 00133 Roma, Italy

³ Dipartimento di Fisica, Università degli Studi di Roma “Tor Vergata”, Via della Ricerca Scientifica 1, 00133 Roma, Italy

⁴ Dipartimento di Fisica, Università degli Studi di Roma “La Sapienza”, Piazzale Aldo Moro 5, 00185 Roma, Italy

Received April 2, 2024; accepted XXX

ABSTRACT

Weakly magnetized neutron stars (WMNS) are complicated sources with challenging phenomenology. For decades, they have been studied via spectrometry and timing. It has been established that the spectrum of WMNSs consists of several components traditionally associated with the accretion disk, the boundary or spreading layer, and the wind and their interactions with each other. Since 2022, WMNSs have been actively observed with the Imaging X-ray Polarimetry Explorer (*IXPE*). Polarimetric studies provided new information about the behavior and geometry of these sources. One of the most enigmatic sources of the class, galactic X-ray burster GX 13+1 was first observed with *IXPE* in October 2023. A strongly variable polarization at the level 2–5% was detected with the source showing a rotation of the polarization angle (PA) that hinted towards the misalignment within the system. The second observation was performed in February 2024 with a complementary observation by *Swift*/XRT. *IXPE* measured an overall polarization degree (PD) of 2.5% and the PA of 24°, and the *Swift*/XRT data helped us evaluate the galactic absorption and fit the continuum. Here we study the similarities and differences between the polarimetric properties of the source during the two observations. We confirm the expectation of the misalignment in the system and the assignment of the harder component to the boundary layer. We emphasize the importance of the wind in the system. We note the difference in the variation of polarimetric properties with energy and with time.

Key words. accretion, accretion disks – polarization – stars: neutron – X-rays: binaries

1. Introduction

Although weakly magnetized neutron stars (WMNS) do not show pulsation or strong orbital variation, they present a complex phenomenology that requires further studies and observations to be explained. The broad class of WMNSs includes sources with a magnetic field of the order of $10^7 - 10^9$ G. These neutron stars accrete matter from the companion via the Roche lobe, and if the accretion rate is high enough to overpower the relatively weak magnetic field, the matter from the accretion disk falls directly onto the equator of the neutron star.

Non-pulsating weakly magnetized neutron stars are traditionally classified into two main groups: Z and atolls, on the basis of the patterns they show on the color-color diagram (CCD) or hardness-intensity diagram (HID). Although the classification is completely phenomenological, objects of these two classes have many other characteristic behavioral properties. For instance, atolls are known to be less bright than the Z-sources: typical luminosity of the atolls is in the range of $10^{36} - 10^{37}$ erg s⁻¹, while Z-sources are among the brightest objects in the X-ray sky with luminosities on the order of 10^{38} erg s⁻¹. However, many features are known to be present in both classes: for example, quasi-periodic oscillations (QPOs) in the Hz and kHz ranges were observed from both Z and atolls sources (van der Klis 1989, 2000). Sources of both classes are observed in both hard and soft states, and the main components of their spectrum are expected to be the same. The spectrum is generally well described by the two main components (see e.g. Revnitvsev et al. 2013). The soft component can be approximated by the multicolor black body

emission of temperature < 1 keV associated with the accretion disk. The harder component most probably comes from Comptonization in a relatively cool plasma (2–3 keV), either a boundary layer between the accretion disk and the surface of the neutron star (Shakura & Sunyaev 1988), or the spreading layer at the neutron star surface (Inogamov & Sunyaev 1999; Suleimanov & Poutanen 2006). Additional features known to the spectrum are the broad Fe emission line associated with the reflection of the spreading layer emission from the accretion disk and sharp absorption lines coming from the absorption of the emission in the wind above the disk.

However, the geometry of the WMNS cannot be fully understood from spectroscopic and time-resolved observations only. Information obtained from variability, and specifically from the QPOs, revealed that the strongest variability is associated with a harder spectral component (Gilfanov et al. 2003; Revnitvsev & Gilfanov 2006; Revnitvsev et al. 2013) originating close to the neutron star surface. Polarimetry brought a new perspective to the problem. For instance, it became possible to distinguish between the boundary and spreading layer emission based on the polarimetric properties of the emission, while spectroscopically they are identical. The boundary layer is expected to have a polarization similar to that of the accretion disk, with the polarization vector lying in the plane of the disk (Chandrasekhar 1960; Loktev et al. 2022), while the polarization of the spreading layer is expected to be perpendicular to the accretion disk (Farinelli et al. 2024). For example, the polarization angle (PA) of the bright Z-source Cyg X-2 (Farinelli et al. 2023) turned out to be consistent with the position angle of the radio jet (which

is likely perpendicular to the accretion disk), implying the origin of the polarization in the spreading layer or from scattering in the accretion disk wind (Tomaru et al. 2024; Nitindala et al., in prep.). In La Monaca et al. (2024), on the other hand, a significant difference between the jet position angle and the PA for Sco X-1 has been observed which implies a more complicated geometry of the source. In the peculiar case of Cir X-1 (Rankin et al. 2024), the variability of the PA with time and hardness supported the idea of a misalignment between the angular momentum of the neutron star and the binary orbital axis. In Z-sources XTE J1701–462 (Cocchi et al. 2023) and GX 5–1 (Fabiani et al. 2023), a significant variation of the polarization between observations in the hard and soft states suggested the change in geometry between states. In atoll sources GX 9+9 (Ursini et al. 2023), 4U 1820–303 (Di Marco et al. 2023a), and 4U 1624–49 (Saade et al. 2024), the strong dependency of the PD on energy supported the separation of the spectrum into two components with the different PAs. These discoveries supported the study of the WMNSs and established the capabilities of polarimetric observations of these sources.

Galactic X-ray burster GX 13+1 was first observed by *IXPE* on 2023 October 17–19 (Bobrikova et al. 2024, hereafter B24). This source is known for the strong wind above the large disk being responsible for a number of absorption lines (Díaz Trigo et al. 2012), the brightness of $0.5L_{\text{Edd}}$ (D’Aí et al. 2014), and an orbital period of 24.5 days, which is very long for a low-mass X-ray binary (Corbet et al. 2010). GX 13+1 presents a classification challenge: it is still debatable whether the source is a Z (see e.g. Saavedra et al. 2023) or an atoll (see e.g. Schnerr et al. 2003).

During the first *IXPE* observation, GX 13+1 presented an enigmatic behavior: the polarimetric properties varied significantly during the observation, while the spectral properties remained almost unchanged. Moreover, GX 13+1 shows a peculiar continuous rotation of the PA by 70° in the two days of observations, together with a change in the pattern of dependence of PD on energy. These two peculiar behaviors left some space for further investigation. Here, we aim to answer some of the open questions and bring a new perspective to the study of GX 13+1.

The remainder of the paper is structured as follows. We introduce the observations performed with *IXPE* and *Swift*/XRT observatories in Sect. 2. In Sect. 3 we present the data analysis. We provide possible interpretations of the results in Sect. 4 and a summary in Sect. 5.

2. Observations

2.1. *IXPE*

IXPE is a joint mission of NASA and the Italian Space Agency (ASI) that was launched on 9 December 2021. The observatory comprises three grazing incidence mirror assembly modules, each having a detector unit (DU), hosting an X-ray detector sensitive to polarization, the Gas Pixel Detector (GPD), in the focal plane (Costa et al. 2001; Baldini et al. 2021). A description of the mission and of the instrument on board is given in Soffitta et al. (2021), and Weisskopf et al. (2022).

IXPE observed GX 13+1 two times, the first one performed in October 2023, reported in B24, and the present standing since 25 February 2024 at 13:34 UTC until 27 February at 12:59 UTC for a total exposure time of about 90 ks in each DU (see Table 1 and the light curve in Fig. 1). Data have been processed for model-independent polarimetric analysis using the *IXPEOBSIM* package version 30.2.1 (Baldini et al. 2022). Spectral and spectro-polarimetric analysis was performed using HEA-

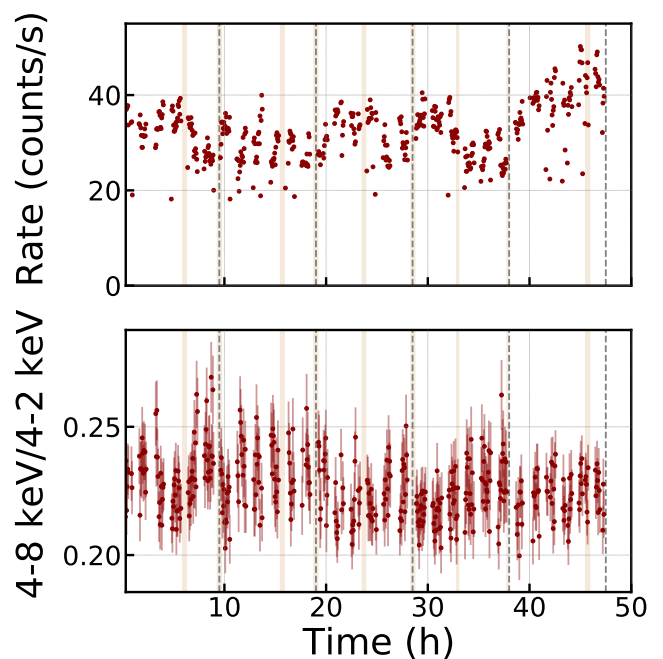


Fig. 1. The *IXPE* light curve obtained combining the 3 DUs (top panel) and the corresponding hardness ratio as a function of time (bottom panel). The data are binned in 200 s. The shaded regions mark the *Swift*/XRT observation periods. Dashed vertical lines illustrate the separation of the observation into five equal time bins of 9.5 h.

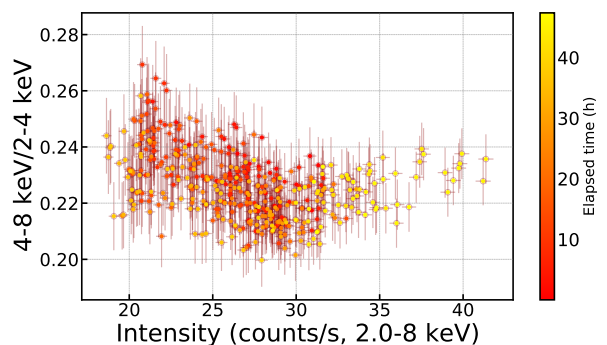


Fig. 2. Hardness-Intensity diagram obtained from *IXPE* data. The data are binned in 200 s.

SOFT version 6.33 and the standard FTOOLS (Nasa High Energy Astrophysics Science Archive Research Center (Heasarc) 2014) with the *IXPE* CALDB released on 28 February 2024. Source photons were selected in a circular region with a radius of $100''$ centered at the source position. As recommended by Di Marco et al. (2023b), given the brightness of the source, the background was not subtracted. The unweighted analysis is performed with *IXPEOBSIM*, while the weighted analysis is adopted for the spectro-polarimetric analysis as suggested by Di Marco et al. (2022a).

2.2. *Swift*/XRT

The Neil Gehrels Swift Observatory (Gehrels et al. 2004) carrying three instruments on board, enables the most detailed observations of gamma-ray bursts to date; the X-ray Telescope (XRT) is one of the instruments on board based on a sensitive, flexible, autonomous X-ray CCD imaging spectrometer. *Swift*/XRT coordinated observations with *IXPE* for GX 13+1 were per-

Table 1. List of *IXPE* and *Swift*/XRT observations: Observation ID, start, stop, and the exposure times are reported.

Observatory	ObsID	Start – Stop	Exposure Time (s)
<i>Swift</i> /XRT-XRT	00036688042	2024-02-26T05:05–2024-02-26T05:27	1366
	00036688043	2024-02-25T13:14–2024-02-25T17:59	892
	00036688044	2024-02-26T13:07–2024-02-26T14:52	1249
	00036688045	2024-02-25T22:53–2024-02-26T00:35	1395
	00036688046	2024-02-26T17:56–2024-02-26T19:30	1311
	00036688047	2024-02-26T08:22–2024-02-26T10:12	1429
	00036688048	2024-02-25T19:28–2024-02-25T21:32	1321
	00036688049	2024-02-26T22:24–2024-02-26T23:59	771
	00036688050	2024-02-27T03:22–2024-02-27T05:14	507
	00036688051	2024-02-27T11:05–2024-02-27T11:29	1443
<i>IXPE</i>	03001101	2024-02-25T13:34–2024-02-27T12:59	90670
			90819
			90799

formed; they are used to monitor the status of the source and obtain spectral information during *IXPE* observation. Given the source brightness, the *Swift*/XRT observations were performed in Windowed Timing mode (WT). Ten *Swift*/XRT pointings covered the *IXPE* observation, as reported in Table 1 and Fig. 1. *Swift*/XRT data were extracted using HEASOFT v6.33 and standard FTOOLS Nasa High Energy Astrophysics Science Archive Research Center (Heasarc) (2014). Source and background extractions were performed using *Swift*/XRT imaging capabilities in an annulus with an inner radius of about 5'' and an outer radius of about 60'' to avoid possible pile-up effects (Romano et al. 2006). The *Swift*/XRT data have been fitted in the energy band 0.7–8 keV to have sufficient statistics in the spectral fits and grouped to have at least 50 counts bin⁻¹. In the analysis, the response matrices released in the HEASARC CALDB on 2023 July 25 have been applied.

3. Data analysis

IXPE observed GX 13+1 for ~90 ks. During the observation, as shown in Fig. 1 (top panel), the source rate was rather stable, with a slight increase at the end of the observation. The source hardness in the *IXPE* data appears to have no strong variations, remaining almost constant throughout the observation; this is in contrast to the previous *IXPE* observation, reported in B24, where a dip corresponding to a slight hardening was present. In Fig. 2, the hardness intensity diagram obtained from the *IXPE* data is reported and shows that hardness did not change by more than 10%.

Swift/XRT observations, covering with short snapshots the *IXPE* observation, allow us to monitor the source spectral state. GX 13+1 studies in the past showed a spectrum that can be well described, as typical in the atoll and Z sources, by a soft diskbb component describing disk emission and Comptonization emission from the spreading/boundary layer that can be described by a bbodyrad component (Díaz Trigo et al. 2012). Better modeling of the hard Comptonization component, e.g., applying compTT or compTB, is not possible due to the limited *IXPE* and *Swift*/XRT energy bands. In the literature, *XMM-Newton* spectra of GX 13+1 are reported showing wind and reflection features (Díaz Trigo et al. 2012), but neither *IXPE* nor *Swift*/XRT allow us to study these features, so in the following the simple spectral model tbabs*(diskbb+bbodyrad) will be applied.

3.1. Spectroscopy

Given the better spectral capabilities, we used *Swift*/XRT data as a driver for spectral modeling and to monitor spectral variations. The analysis is carried out in the energy band 0.7–8 keV, best-fit values are reported for each observation in Table 2 with uncertainties at the 68% confidence level (CL), and ObservationIDs are ordered by the observation date to show the time evolution of the spectral model.

In the spectral analysis, the *Swift*/XRT data are fitted with the model: tbabs*(diskbb+bbodyrad). In the different pointings, it is possible to observe that the absorption is in average $\sim 4.7 \times 10^{22}$ cm⁻², while the disk temperature ranges between 0.7–1.1 keV, about the bbodyrad component – which in our case is used to describe a Comptonization emission from the boundary layer – the temperature ranges in the ~ 1.3 –1.8 keV. The flux is in the range $\sim (4$ – $6) \times 10^{-9}$ erg cm⁻² s⁻¹ except in the last pointing where it reaches the highest value of $\sim 8 \times 10^{-9}$ erg cm⁻² s⁻¹. The hardness, reported in Table 2 is defined as

$$\text{Hardness} = \frac{\text{Flux}_{0.7-3 \text{ keV}} - \text{Flux}_{3-8 \text{ keV}}}{\text{Flux}_{0.7-8 \text{ keV}}} \quad (1)$$

and the spectral models report an almost constant hardness value except for the case of ObservationID 00036688045 where the flux is at a minimum and there is a slight hardening, but this *Swift*/XRT observation (third snapshot) is performed mainly during an *IXPE* occultation period. Thus, the *IXPE* data are not affected by this slight hardening, while the other snapshots confirm the *IXPE* result of an almost constant hardness ratio during observation. In the following analysis, for the spectro-polarimetric study, this ObservationID will be excluded, while the other ones will be used in the joint fit with the *IXPE* data.

Taking into account the whole *IXPE* observation, and the *Swift*/XRT spectra, except the ObservationID 00036688045, we obtain a good joint spectrum model. The best-fit parameters are reported in Table 3 and Fig. 3. To take into account the calibration uncertainties in the *IXPE* data, (see, e.g., Di Marco et al. 2022b), we left the gain slope and offset of the *IXPE*-DUs free to vary.

The joint fit confirms the result expected for the average model from several *Swift*/XRT snapshots. In the following for the spectro-polarimetric analysis, the spectral model will be frozen to the present one. The *IXPE* gain correction is at level of 0.95 for the slope in all the three DUs and the offset in the range 70–100 eV.

Table 2. Best-fit parameters for the spectral model $\text{TBabs}^*(\text{diskbb}+\text{bbodyrad})$ as obtained by the different *Swift*/XRT spectra.

ObsID	tbabs		diskbb		bbodyrad		$\chi^2/\text{d.o.f.}$	Flux _{2–8 keV} (10^{-9} erg cm $^{-2}$ s $^{-1}$)	Hardness
	N_{H} (10^{22} cm 2)	kT_{in} (keV)	norm	kT_{bb} (keV)	norm				
00036688043	$4.54^{+0.18}_{-0.14}$	$1.1^{+0.6}_{-0.2}$	250^{+260}_{-160}	$1.5^{+0.6}_{-0.1}$	100^{+60}_{-90}	0.93	6.0	0.35	
00036688048	4.52 ± 0.10	[1.0]	290 ± 19	1.52 ± 0.04	120 ± 12	0.91	5.9	0.37	
00036688045	5.71 ± 0.19	0.67 ± 0.05	1100 ± 400	1.57 ± 0.04	100 ± 10	1.13	4.1	0.45	
00036688042	5.0 ± 0.2	$0.70^{+0.10}_{-0.07}$	1000^{+700}_{-400}	$1.41^{+0.06}_{-0.04}$	150 ± 30	1.06	5.9	0.38	
00036688047	$4.62^{+0.14}_{-0.18}$	$0.88^{+0.38}_{-0.10}$	500 ± 300	$1.38^{+0.18}_{-0.05}$	200^{+40}_{-100}	1.12	6.0	0.36	
00036688044	$4.67^{+0.17}_{-0.15}$	$0.98^{+0.39}_{-0.15}$	400^{+300}_{-200}	$1.46^{+0.31}_{-0.09}$	130^{+60}_{-100}	1.04	5.9	0.33	
00036688046	$4.9^{+0.3}_{-0.2}$	$0.70^{+0.11}_{-0.08}$	1100^{+900}_{-600}	$1.29^{+0.06}_{-0.04}$	230^{+40}_{-50}	1.10	5.0	0.33	
00036688049	4.3 ± 0.3	$1.0^{+0.6}_{-0.2}$	320^{+630}_{-260}	$1.7^{+1.3}_{-0.1}$	80^{+65}_{-75}	1.16	5.4	0.34	
00036688050	5.7 ± 0.4	$0.66^{+0.12}_{-0.09}$	1800^{+2000}_{-1000}	$1.46^{+0.11}_{-0.08}$	130 ± 40	0.92	4.7	0.36	
00036688051	$4.70^{+0.12}_{-0.09}$	$1.13^{+0.19}_{-0.16}$	310^{+200}_{-120}	$1.77^{+0.28}_{-0.17}$	80^{+50}_{-40}	1.16	7.9	0.35	

Notes. The fits are performed in the energy band 0.7–8.0 keV. Errors correspond to the 68% CL. The reported flux has a typical uncertainty of the order of 0.3×10^{-9} . The hardness is defined as in Eq. (1).

Table 3. Best-fit parameters of the model $\text{const}^*\text{tbabs}^*(\text{diskbb}+\text{bbodyrad})$ for the joint *Swift*/XRT and *IXPE* spectra.

Model	Parameter	Value
tbabs	N_{H} (10^{22} cm 2)	$4.45^{+1.0}_{-0.05}$
diskbb	kT_{in} (keV)	$0.88^{+0.10}_{-0.07}$
	norm	390^{+140}_{-130}
bbodyrad	kT_{bb} (keV)	$1.33^{+0.13}_{-0.14}$
	norm	228^{+20}_{-8}
const	<i>Swift</i> /XRT/XRT	[1]
	<i>IXPE</i> -DU1	0.722 ± 0.003
	<i>IXPE</i> -DU2	0.686 ± 0.003
	<i>IXPE</i> -DU3	0.658 ± 0.003
$\chi^2/\text{d.o.f.}$		991/956=1.04
	Flux (10^{-9} erg cm $^{-2}$ s $^{-1}$)	
	2–8 keV	6.0
	diskbb	1.3
	bbodyrad	4.7

Notes. Errors correspond to the 68% CL.

3.2. Polarimetry

Spectroscopy revealed that neither the light curve nor the hardness have strong dips or features that would suggest separating the observation into several parts to be studied independently. To study the time variability of the polarimetric properties, we followed the same approach as in B24 and split this new *IXPE* observation into five equal time bins spanning 9.5 h. The results are reported in Fig. 4.

Time dependence of the polarimetric properties showed a hint for variability in PD, completely different with respect to the rotation we observed in the first *IXPE* observation. We found it useful to proceed with analyzing the observation as a whole, since there are no clear trends. Next, we study the dependence of the polarimetric properties on energy; the results are reported in Fig. 5. The polarization shows a hint for an energy dependence, but the significance for this trend is less than 2σ , see later in the spectro-polarimetric analysis. The average polarization, in energy and time, resulting from this observation is $\text{PD}=2.6\% \pm 0.5\%$ with the $\text{PA} = 23^\circ \pm 5^\circ$ at a significance level of 5.2σ , corresponding to a secure detection at $\text{CL} > 99.9999\%$.

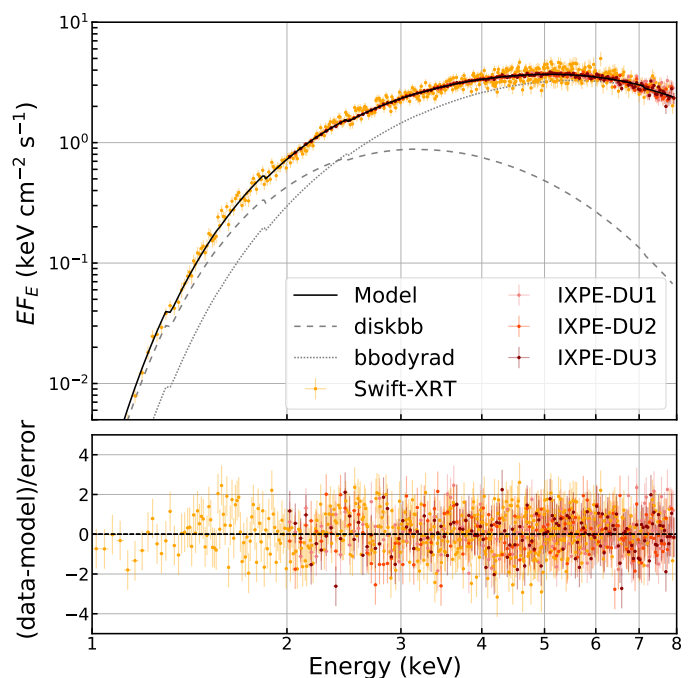


Fig. 3. Joint spectral fit *Swift*/XRT and *IXPE* in the 1–8 keV energy range. In the top panel the spectra of each telescope are reported in EF_E units, in the bottom panel the residuals are shown.

3.3. Spectro-polarimetry

To study the polarization of the different spectral components, we used the results from the spectral analysis to freeze the spectral model in the spectro-polarimetric analysis. First, instead of studying the polarization of each spectral component independently, we applied the `polconst` model to the entire continuum model to confirm model-independent analysis. The result is an average PD of $2.4\% \pm 0.3\%$ with the $\text{PA}=28^\circ \pm 3^\circ$, fully compatible with the model-independent analysis. Then we replaced the `polconst` model with `pollin` to get a quantitative estimation of the dependency of polarization on energy. We obtained non-zero slopes for PA and PD, but they are compatible with zero within a 2σ level. Finally, we applied a model with different polarizations for each spectral component, obtaining a PD of $6.1\% \pm 1.6\%$ and a PA of $41^\circ \pm 7^\circ$ for the `diskbb` component, and a PD of $1.6\% \pm 0.9\%$ with PA of $6^\circ \pm 10^\circ$ for the `bbodyrad`.

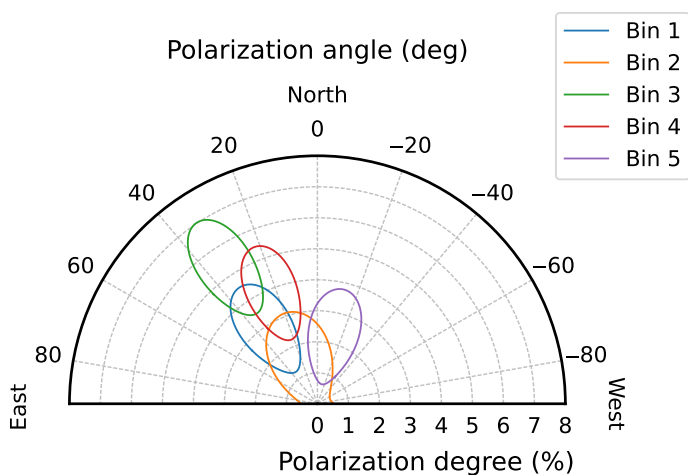
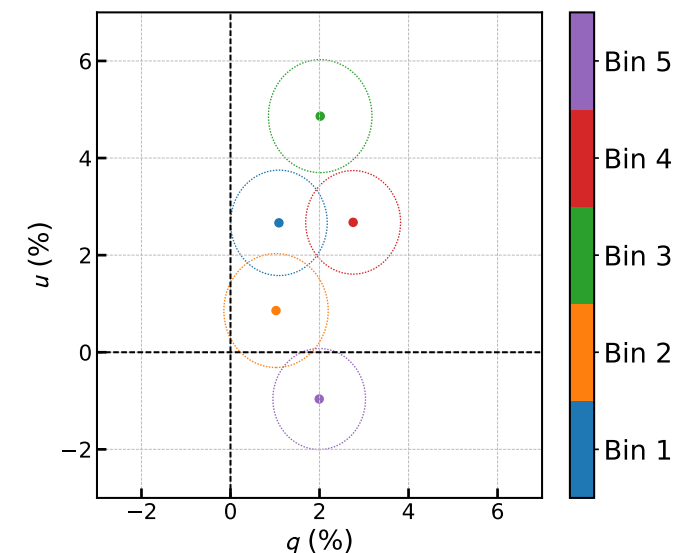


Fig. 4. Time dependence of the normalized Stokes parameters q and u (top), and of the PD and PA (bottom) obtained by the *pcube* algorithm using the data separated into 9.5 h time bins. The confidence regions are reported at 68%.

The results of the spectro-polarimetric analysis are summarized in Table 4, the best-fit plots for the spectro-polarimetric analysis are reported for the I , Q , and U Stokes parameters are reported in Fig. 6.

4. Discussion

Although interesting as a single observation, the results reported in this article provide the most information when compared to the results of the October observations reported in B24. Overall, in October *IXPE* measured a PD of $\sim 1.4\%$ and a PA of $\sim -2^\circ$, significantly different from the current results. However, the reason for the depolarization in the first observation was fast variability in the PA. In B24, the observation was separated into the pre-dip, dip, and post-dip states. The results for the dip were poorly constrained, but the other two are presented in Fig. 7 and compared to the results of the current observation. We note that the current observation is similar in PA to the post-dip state of B24. The lower PD in the entire current observation most probably comes from averaging the entire observation in time and

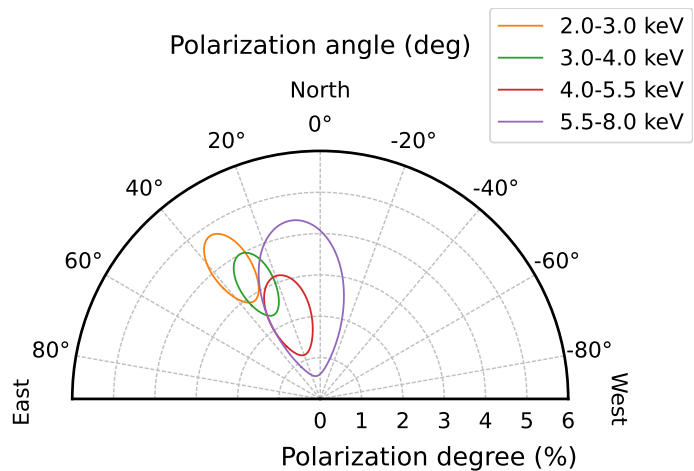
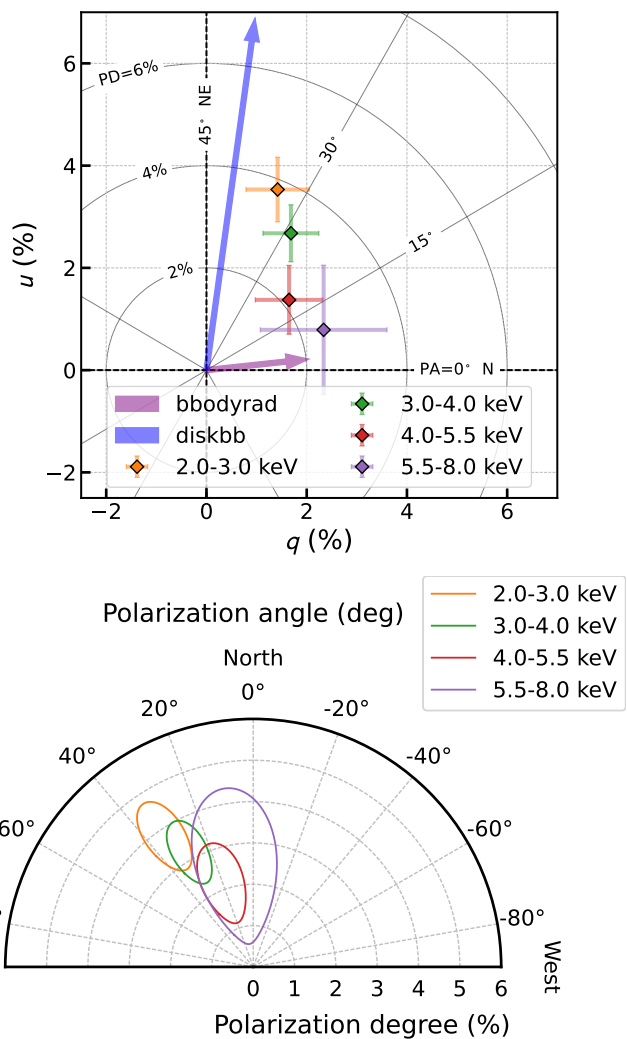


Fig. 5. Energy resolved normalized Stokes parameters q and u (top), and PD and PA (bottom) obtained by the *pcube* algorithm using the reported energy bins for the time-averaged data. The confidence regions are reported at 68% CL. The vectors correspond to the best-fit polarization parameters of the *diskbb* and *bbodyrad* components, respectively, as obtained in the spectro-polarimetric analysis and reported in Table 4.

energy, as for the previous one. In Fig. 4, the Bin 3, for instance, shows a polarization within errors similar to the one measured after the dip in B24.

Both HID and the shape of the spectrum confirm that GX 13+1 was in a soft state throughout the observation. We do not see any significant change of state in the *IXPE* and *Swift*/XRT energy bands, although, in the last part of the observation, the flux rises, which is a sign of the source going into an even softer state. If we look at the HID of the source in the October observation (B24, Figure 2), we see that the source is almost in the same state, except for the dipping period. In this new observation, since simultaneous *Swift*/XRT observations offer a better spectral capability than *IXPE*, the spectral modeling and decomposition into two main components are better determined, allowing for a better spectro-polarimetric analysis.

The light curve does not show any peculiar variability: unlike the one from the October observation, the current one has no strong dips or rapid changes, and neither does the hardness

Table 4. *IXPE* spectro-polarimetric fit of the Stokes parameters I , Q , and U using the spectral model from Table 3.

Model	PD/ A_1 (%)	A_{slope} (% keV $^{-1}$)	PA/ ψ_1 (deg)	ψ_{slope} (deg, keV $^{-1}$)	$\chi^2/\text{d.o.f.}$
tbabs*(diskbb+bbodyrad)*polconst	2.4 ± 0.3	–	28 ± 3	–	243/250=0.97
tbabs*(diskbb+bbodyrad)*pollin	3.8 ± 0.8	-0.5 ± 0.3	28 ± 3	-8 ± 4	234/248=0.94
tbabs*(diskbb*polconst	6.5 ± 1.6	–	41 ± 7	–	235/248=0.95
+bbodyrad*polconst)	1.6 ± 0.7	–	3 ± 13	–	

Notes. Errors correspond to 68% CL.

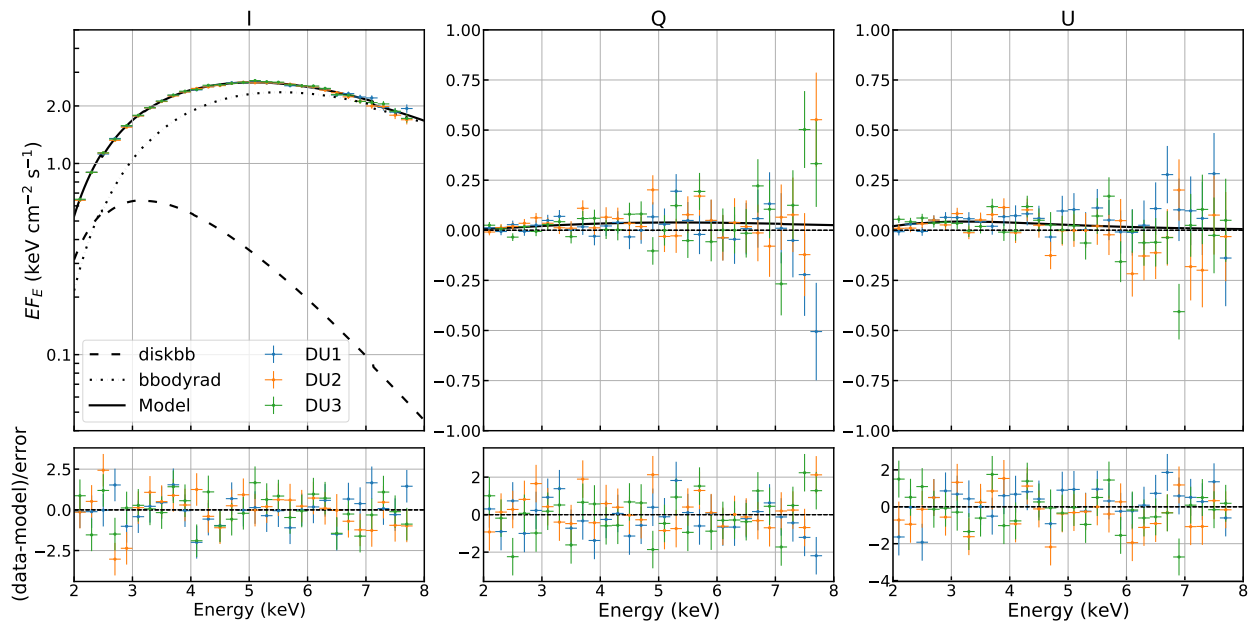


Fig. 6. Spectral energy distribution of GX 13+1 in EF_E representation as observed by *IXPE*. The left, middle, and right panels are for the Stokes parameters I , Q , and U , respectively. The fit is performed in the 2–8 keV energy band using the three *IXPE* detectors and applying the model $\text{tbabs}^*(\text{diskbb}^*\text{polconst}+\text{bbodyrad}^*\text{polconst})$. The total model is shown with the solid black line, while the diskbb and bbodyrad with the dashed and dotted lines, respectively. The lower sub-panels show the residuals between the data and the best fit. In the joint spectral fit, we apply a rebinning to have at least 50 counts per bin as in *Swift*/XRT, while for the spectro-polarimetric analysis, a constant grouping is applied to have energy bins of 200 eV.

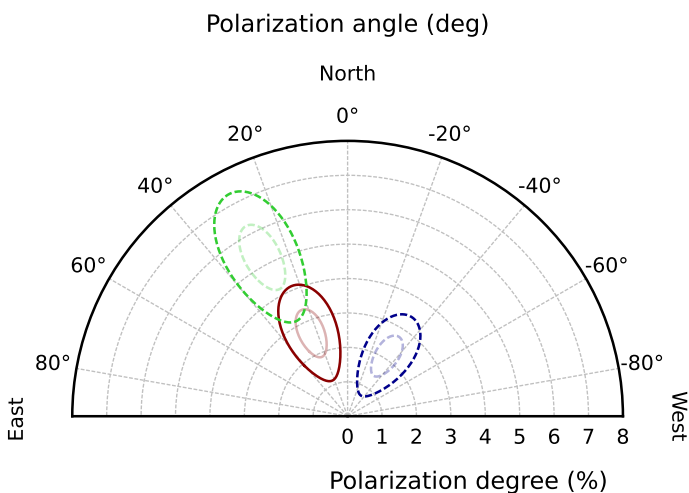


Fig. 7. Average polarization in the 2–8 keV energy band for the pre-dip (dashed blue lines) and post-dip (dashed green lines) of the first observation of GX 13+1, and for the new observation (solid dark red lines). The contours correspond to the 68% and 99% CL. A significant detection of polarization at 5.2σ is obtained in the new observation with the PA aligned with the post-dip reported in B24.

ratio. Despite this constant hardness, we attempted to study the possible variation in 9.5 h equal time bins similarly to B24. This analysis reports a hint for a variation in PD in Fig. 4, in particular is interesting that in Bin 5, corresponding to a softening of GX 13+1 there is a lower polarization and an indication for a possible rotation with respect to the other 4 time bins. The clear rotation of PA observed during the first observation is not present this time, but the PA appears to have remained aligned with the post-dip polarization measured in B24. If we compare the positions of the points on the (q, u) plane with those obtained from the October 2023 observation (Figure 7 in B24), we see a different pattern, but the points are still in the I or IV quadrant. The biggest difference is in order: in October, we saw the points following the straight line path, but here the variability shows a different pattern.

On the basis of the almost constant hardness and flux, we decided to examine the observation as a whole and study the polarization as a function of energy. As presented in Table 4, the slopes of the pollin model are consistent with zero at the 2σ level, so we can only report a hint towards the dependence of PA and PD on energy. However, it is interesting to notice that the spectro-polarimetric analysis assigned very different PAs to the two main continuum components. Figure 5(top) illustrates this decomposition: while the PD of the disk is rather high, the contribution of the disk to the total spectrum is low, and it be-

comes even lower with energy, as the Comptonized component dominates more and more. The most interesting part here is the unusual difference in PA of the two components of 30° – 40° . It is possible to observe an indication of this in the energy-resolved analysis with the 2–3 keV bin near to the arrow corresponding to the DISKBB component polarization, and the 5.5–8.0 keV energy bin approaching the arrow representing the polarization of the BBODYRAD component.

From the aligned systems, we expect the polarization vectors of the emission coming from the disk and the Comptonized component to be either nearly parallel or perpendicular to each other. Hence, we expect some misalignment in the system that could support this difference in the PA. Another thing to notice is a very high PD of the disk component: as was mentioned in Loktev et al. (2022), we do not expect a polarization higher than 4% in the *IXPE* energy range even for the highest inclination. This value is compatible with the spectro-polarimetric results at 90% CL. However, knowing that the source is likely to have an inclination lower than 80° (Díaz Trigo et al. 2012; Tomaru et al. 2020), we need to add the scattering of the disk emission in the wind to reach the PD of 6.5%. We assume that the Comptonized component comes from the boundary layer, as it is expected to align in PA with the disk emission, and the difference in PAs is less than 45° .

In search of a source of misalignment, we looked at the previous observations of *IXPE*. It is possible (although unexpected) that, similar to the Cir X-1 (Rankin et al. 2024), the rotation axis of the neutron star is slightly misaligned from the rotation axis of the binary system. The boundary layer would then be dragged out of the disk plane by the motion of the star. Another option would be the peculiar geometry of the wind in the system.

Finally, we want to address the significant difference between the two observations of GX 13+1. The object was in the same spectral state but half an orbit away from the previous observation, when the source clearly showed a rotation of the PA with time. However, in February 2024, there was no clear monotonic change in the PA, while we still see variations in the PA. One possibility is that the mechanism responsible for the dip in the light curve during the first observation was also responsible for the rotation of the PA. However, this mechanism is unknown. What we can address is that from this new observation, it appears that the PA remained aligned with the one observed in the end of the previous observation. Then, at the end of the present *IXPE* pointing, when the flux grows and the source goes into a softer state, the PD decreases and rotates to a PA similar to the one we observed in October before the dip. This could suggest, similarly to what we observed in Cir X-1, a variation of the PA with the state of the source. This could mean a variation of the geometry of the hot region in different states; this can also be confirmed by the indication we obtained in the October 2023 observation when the energy dependence of the polarization changed before and after the dip going from an energy-dependent behavior, as observed e.g. for 4U 1820–30 (Di Marco et al. 2023a), into a constant polarization with energy, as observed, e.g., for Sco X-1 in La Monaca et al. (2024). Present data do not allow for a clear statement on this, but we hope in the future we could obtain further observations to improve the significance for a detailed analysis of the polarization along the states of atoll and Z sources.

A further point is the contribution of the wind, as we are unaware of the wind behavior during both observations, we can also assume that it could be responsible for the differences in polarimetry, yet we have no way to support this claim.

5. Summary

We analyzed the observation of GX 13+1 carried out simultaneously by *IXPE* and *Swift*/XRT. In this article, we report the highly significant detection of polarization from this source in the soft state. Spectroscopic analysis showed that the spectrum is close to that in Díaz Trigo et al. (2012), and the hardness of the emission confirmed the lower left banana state, as well as the further softening of the spectrum at the end of this new observation. We used a diskbb model for the softer disk emission, and the bbodyrad model to approximate the harder component associated with the spreading or boundary layer. The polarimetric analysis provided the overall PD of the source during the observation at 2.5% at $>5\sigma$ CL, and a PA at 24° . We also saw a marginally significant decrease in PD and PA with energy. The same trend was confirmed in the spectro-polarimetric analysis, which showed that the softer component is stronger polarized than the harder component with the PA differing by $\sim 40^\circ$. The results of the spectro-polarimetric analysis using XSPEC performed under the assumption of one overall polarization model agreed with the pcube polarimetric results.

We studied the differences and similarities between the first (B24) and the second observations of GX 13+1 by *IXPE*. Our main conclusion is that we saw a significantly higher overall polarization in the second observation, even though the source was in the same state during both observations. The depolarization comes from the variability of polarimetric properties, which was larger in the first observation. We discussed possible reasons for the different polarimetric behavior in the two observations.

Acknowledgements. This research used data products provided by the IXPE Team (MSFC, SSDC, INAF, and INFN) and distributed with additional software tools by the High-Energy Astrophysics Science Archive Research Center (HEASARC), at NASA Goddard Space Flight Center (GSFC). The Imaging X-ray Polarimetry Explorer (IXPE) is a joint US and Italian mission. The Italian contribution is supported by the Italian Space Agency (Agenzia Spaziale Italiana, ASI) through contract ASI-OHBI-2022-13-I.0, agreements ASI-INAf-2022-19-HH.0 and ASI-INFN-2017.13-H0, and its Space Science Data Center (SSDC) with agreements ASI-INAf-2022-14-HH.0 and ASI-INFN 2021-43-HH.0, and by the Istituto Nazionale di Astrofisica (INAF) and the Istituto Nazionale di Fisica Nucleare (INFN) in Italy. We thank the *Swift* Project Scientists for approving our DDT request to observe GX 13+1. This research has been supported by the Finnish Cultural Foundation grant 00240328 (AB) and the Academy of Finland grant 333112 (AB, JP, SVF, VL). ADM, FLM are partially supported by MAECI with grant CN24GR08 “GRBAXP: Guangxi-Rome Bilateral Agreement for X-ray Polarimetry in Astrophysics”.

References

- Baldini, L., Barbanera, M., Bellazzini, R., et al. 2021, *Astroparticle Physics*, 133, 102628
- Baldini, L., Bucciantini, N., Di Lalla, N., et al. 2022, *SoftwareX*, 19, 101194
- Bobrikova, A., Forsblom, S. V., Di Marco, A., et al. 2024, arXiv e-prints, arXiv:2401.13058
- Chandrasekhar, S. 1960, *Radiative Transfer* (New York: Dover)
- Cocchi, M., Gnarini, A., Fabiani, S., et al. 2023, *A&A*, 674, L10
- Corbet, R. H. D., Pearlman, A. B., Buxton, M., & Levine, A. M. 2010, *ApJ*, 719, 979
- Costa, E., Soffitta, P., Bellazzini, R., et al. 2001, *Nature*, 411, 662
- D’Ái, A., Iaria, R., Di Salvo, T., et al. 2014, *A&A*, 564, A62
- Di Marco, A., Costa, E., Muleri, F., et al. 2022a, *AJ*, 163, 170
- Di Marco, A., La Monaca, F., Poutanen, J., et al. 2023a, *ApJ*, 953, L22
- Di Marco, A., Muleri, F., Fabiani, S., et al. 2022b, in *Proc. SPIE*, Vol. 12181, Space Telescopes and Instrumentation 2022: Ultraviolet to Gamma Ray, ed. J.-W. A. den Herder, S. Nikzad, & K. Nakazawa, 121811C
- Di Marco, A., Soffitta, P., Costa, E., et al. 2023b, *AJ*, 165, 143
- Díaz Trigo, M., Sidoli, L., Boirin, L., & Parmar, A. N. 2012, *A&A*, 543, A50
- Fabiani, S., Capitanio, F., Iaria, R., et al. 2023, *A&A*, in press, arXiv:2310.06788
- Farinelli, R., Fabiani, S., Poutanen, J., et al. 2023, *MNRAS*, 519, 3681
- Farinelli, R., Waghmare, A., Ducci, L., & Santangelo, A. 2024, arXiv e-prints, arXiv:2401.16239

- Gehrels, N., Chincarini, G., Giommi, P., et al. 2004, *ApJ*, 611, 1005
- Gilfanov, M., Revnivtsev, M., & Molkov, S. 2003, *A&A*, 410, 217
- Inogamov, N. A. & Sunyaev, R. A. 1999, *Astronomy Letters*, 25, 269
- La Monaca, F., Di Marco, A., Poutanen, J., et al. 2024, *ApJ*, 960, L11
- Loktev, V., Veledina, A., & Poutanen, J. 2022, *A&A*, 660, A25
- Nasa High Energy Astrophysics Science Archive Research Center (Heasarc).
2014, HEASoft: Unified Release of FTOOLS and XANADU, Astrophysics
Source Code Library, record ascl:1408.004
- Rankin, J., La Monaca, F., Di Marco, A., et al. 2024, *ApJ*, 961, L8
- Revnivtsev, M. G. & Gilfanov, M. R. 2006, *A&A*, 453, 253
- Revnivtsev, M. G., Suleimanov, V. F., & Poutanen, J. 2013, *MNRAS*, 434, 2355
- Romano, P., Campana, S., Chincarini, G., et al. 2006, *A&A*, 456, 917
- Saade, M. L., Kaaret, P., Gnarini, A., et al. 2024, *ApJ*, 963, 133
- Saavedra, E. A., García, F., Fogantini, F. A., et al. 2023, *MNRAS*, 522, 3367
- Schnerr, R. S., Reerink, T., van der Klis, M., et al. 2003, *A&A*, 406, 221
- Shakura, N. I. & Sunyaev, R. A. 1988, *Advances in Space Research*, 8, 135
- Soffitta, P., Baldini, L., Bellazzini, R., et al. 2021, *AJ*, 162, 208
- Suleimanov, V. & Poutanen, J. 2006, *MNRAS*, 369, 2036
- Tomaru, R., Done, C., & Odaka, H. 2024, *MNRAS*, 527, 7047
- Tomaru, R., Done, C., Ohsuga, K., Odaka, H., & Takahashi, T. 2020, *MNRAS*,
497, 4970
- Ursini, F., Farinelli, R., Gnarini, A., et al. 2023, *A&A*, 676, A20
- van der Klis, M. 1989, *ARA&A*, 27, 517
- van der Klis, M. 2000, *ARA&A*, 38, 717
- Weisskopf, M. C., Soffitta, P., Baldini, L., et al. 2022, *JATIS*, 8, 026002